Preparation and Properties of Castor Oil-Based Polyurethane/α-Zirconium Phosphate Composite Films

Jun Ma, Changhua Liu, Rui Li, Haixia Wu, Lina Zhu, Yajuan Yang

College of Chemistry and Chemical Engineering, Southwest University, 400715, Chongqing, China

Received 26 April 2010; accepted 26 October 2010
DOI 10.1002/app.33669
Published online 8 March 2011 in Wiley Online Library (wileyonlinelibrary.com).

ABSTRACT: Novel castor oil-based polyurethane/α-zirconium phosphate (PU/α-ZrP) composite films with different α-ZrP loading (0–1.6 wt %) and different NCO/OH molar ratios were synthesized by a solution casting method. The characteristic properties of the PU/α-ZrP composite films were examined by Fourier transform infrared spectroscopy (FTIR), thermal gravimetric analysis (TGA), differential scanning calorimetry (DSC), X-ray diffraction (XRD), scanning electron microscopy (SEM), transmission electron microscopy (TEM), and tensile testing. The results from Fourier transform infrared spectroscopy indicated that strong intermolecular hydrogen bonding formed between α-ZrP and PU, XRD and SEM results revealed that the α-ZrP particles were uniformly distributed in the PU matrix at low loading, and obvious aggregation existed at high loading. Because of hydrogen bonding interactions, the maximum values of tensile strength were obtained with 0.6 wt % α-ZrP loading and 1.5 of NCO/OH molar ratio in the matrix. Evidence proved that the induced α-ZrP used as a new filler material can affect considerably the mechanical and thermal properties of the composites. © 2011 Wiley Periodicals, Inc. J Appl Polym Sci 121: 1815–1822, 2011

Key words: α-zirconium phosphate (α-ZrP); castor oil-based polyurethane (PU); composite; interaction; mechanical property

INTRODUCTION

Bio-based materials obtained from renewable resources are receiving considerable attention for an increasing amount of applications[1–4] from a social, environmental, and energy standpoint, with the increasing emphasis on issues concerning waste disposal and depletion of nonrenewable resources. Vegetable oils are most abundant, annually renewable natural resources available in large quantities from various oilseeds, such as castor, palm, and canola oils;[5–9] they are relatively low cost materials which offer the possibility of biodegradation. Castor oil is a relatively inexpensive source of secondary hydroxyl groups and a triglyceride of fatty acids with ricinoleic acid being the major constituent,[10] and it has been used as a polyol to synthesize cost-effective and biodegradable polyurethane. However, disadvantages with the use of castor oil include low hydroxyl number leading to inherently low modulus materials, a sluggish rate of curing of the secondary hydroxyl groups[11] and structural irregularity due to steric hindrance offered by the long pendant fatty acid chains during urethane formation, resulting in low tensile strength.[12] To improve the mechanical strength of castor oil based polyurethane, various types of fillers, like clay,[13] CNTs,[14] TiO_2,[15] silicate[16] used as an effective strategy have been incorporated into PU to prepare composites. The results demonstrated that uniform dispersion of fillers in PU matrix significantly improved the performance of the composites.

The α-zirconium phosphate (α-ZrP) $Zr(HPO_4)_2{\cdot}H_2O$ has been used as inorganic filler in some composite films researches, such as Poly(vinyl alcohol) (PVA)[17] and starch[18] intensively due to controlled surface, excellent functionalities, high aspect ratios, and perfect particle sizes and so on,[19–22] most of which are superior to natural layered fillers (i.e., montmorillonite). This compound has the layered structure being similar to montmorillonite clay. However what the most importance is that the layers are formed by zirconium atoms between of which are connected by the oxygen atoms of the phosphate groups and each phosphate molecule contributes three oxygen atoms to the formation of these layers, leaving one OH group pointing into the interlayer space.[23] It is well known that the urethane linkages polyurethane can serve as H-bond acceptor and donor. The OH groups onto the surface of the layers can improve the compatibility with cast oil-based polyurethane. This would endow the composites with better properties due to the formation of stronger hydrogen bonding, resulting in stronger adhesion between α-ZrP and PU matrix.

So, these considerations have prompted us to make elaborate and critical study of the effect of

Correspondence to: C. Liu (chliu@swu.edu.cn).

α-ZrP on the structure and physical properties of the PU. In the work, the key interaction between α-ZrP and PU was discussed. The structure, thermal and mechanical properties of the composite films are studied by Fourier transform infrared (FTIR) spectroscopy, wide-angle X-ray diffraction (XRD), scanning electron microscope (SEM), transmission electron microscopy (TEM), thermogravimetric analysis (TGA), differential scanning calorimetry (DSC), and tensile testing.

EXPERIMENTAL

Materials

All the chemicals and reagents used were of analytical grade. $ZrOCl_2.8H_2O$ was provided by Kelong Chemical Co. (Chongqing, China). 2,4-Toluene diisocyanate (2,4-TDI) was purchased from Kelong Chemical Co. (Chongqing, China) and used without further purification. Castor oil, chemical grade with a 4.94 wt % content of hydroxyl groups and hydroxyl value of 163, was obtained from Daxing Chemical Co. (Ningbo, China) and dehydrated at 100°C under 20 mmHg for 1 h.

Preparation of layered α-zirconium phosphate

α-ZrP was synthesized according to previous study.[24] In detail, a sample of 10.0 g of $ZrOCl_2.8H_2O$ was refluxed with 100.0 mL of 12.0*M* H_3PO_4 in a Pyrex glass flask at 100°C for 24 h. After the reaction, the product was washed and collected by centrifugation three times. Then, the α-ZrP was dried at 60°C for 24 h. The dried α-ZrP was ground with a mortar and pestle into fine powders.

Synthesis of PU/α-ZrP composites

PU/α-ZrP composite films were prepared by a prepolymer mixing process. PU prepolymer was synthesized in a 250-mL three-necked flask equipped with a condenser, thermostat, mechanical stirrer and a pressure equalizing dropping funnel. 30.0 g of 2, 4-TDI was firstly charged into the flask. Totally, 59.0 g of castor oil was dropped into the flask within 40 min and stirred at 60°C for 2 h to get the PU prepolymer. The value of [NCO]/[OH] was predetermined theoretically to be 1.05. After the preparation of the prepolymer, it was cooled to room temperature. Then, 3.0 g of PU prepolymer was mixed with 0.25 g of 1, 4-butanediol as chain-extending agent in tetrahydrofuran (THF).[25] At the same time, a stoichiometric amount of α-ZrP was added into the solution. The composite was cast onto glass plate after stirred at room temperature for 1 h. After slow solvent evaporation at room temperature in atmosphere, it was cured at 80°C for 4 h. The films were vacuum-dried at room temperature for three days and then were used for the measurements.[25] By adjusting α-ZrP loading to 0, 0.2, 0.4, 0.5, 0.6, 0.7, 0.8, 1.0, and 1.6 wt %, respectively, a series of the films with a thickness of around 0.1 mm were prepared and coded as PU-ZrPn (where *n* represents 10 times of α-ZrP loading levels). To serve as experimental controls, the neat PU film was obtained through the same fabrication process, which was coded as PU. The codes of samples were listed in Table I.

The composite films with different NCO/OH molar ratios were prepared by a similar process and coded as PU-ZrP-B1, PU-ZrP-B2, PU-ZrP-B3, PU-ZrP-B4, PU-ZrP-B5 with NCO/OH molar ratio from 1.8 to 0.8. NCO/OH molar ratios were regulated by the changes of 1, 4-butanediol content, while keeping the loading levles of α-ZrP constant at 0.6 wt %. The composites are listed in Table I.

Apparatus

Fourier transform infrared (FTIR) spectroscopy

FTIR spectroscopy of the complex was recorded with a Nicolet 170SX (Madison, WI) Fourier transform infrared spectrometer in the wavelength range of 4000-600 cm^{-1} in the attenuated total reflection mode.

X-ray diffraction

X-ray diffraction (XRD) patterns of the samples were carried out with a XRD-3D, PuXi (Beijing, China) X-ray diffractometer under the following conditions: Nickel filtered Cu*K*α radiation ($\lambda = 0.15406$ nm) at a voltage of 36 kV and current of 20 mA. The scanning rate was 4°/min in the angular range of 3–50° (2θ).

Scanning electron microscopy

The PU-ZrPn complex films were fractured in liquid nitrogen and the cross sections were mounted on SEM stubs with double-sided adhesive carbon tape, and then coated with gold in a 13.3 Pa vacuum degree. A scanning electron microscope (JSM-6460LV, Japan) was used to observe the morphologies of cross sections of the films at an accelerating voltage of 20 kV.

Transmission electron microscopy

TEM micrographs were obtained with a transmission electron microscope (JEM-100CXII, Japan) at an accelerating voltage of 80 kV. Ultrathin sections were microtomed at room temperature.

TABLE I
Codes of the Samples, Mechanical Properties of all the Composite Films and the Thermal Analysis of PU, PU-ZrP4, PU-ZrP6, PU-ZrP8, and PU-ZrP16 Composite Films Measured from the DTG and DSC; the Results of XRD Calculated Crystal Size *D* of (001) Direction for α-ZrP in the Composites

Compound code	Feed composition (wt %)			Thermal analyses			Mechanical properties		
	PU	α-ZrP	NCO/OH molar ratio	T_{max} (°C)	IPDT (°C)	T_g (°C)	σ_b (MPa)	ε_b (%)	*D* (nm) ((001) direction for α-ZrP)
PU	100	0.0	1.05	311.60	297.80	18.40	6.91	430.14	
PU-ZrP2	99.8	0.2	1.05	311.90	319.00	20.60	14.97	408.21	58.91
PU-ZrP4	99.6	0.4	1.05	309.90	333.23	25.68	15.09	378.79	31.20
PU-ZrP5	99.5	0.5	1.05	311.40	313.20	24.12	23.08	290.47	30.59
PU-ZrP6	99.4	0.6	1.05	320.30	312.60	23.79	25.03	279.98	33.45
PU-ZrP7	99.3	0.7	1.05				23.44	283.46	38.89
PU-ZrP8	99.2	0.8	1.05				17.77	302.14	41.11
PU-ZrP10	99.0	1.0	1.05				13.94	335.91	
PU-ZrP16	99.8	1.6	1.05				9.12	379.47	
PU-ZrP-B1	99.4	0.6	0.80				23.36	296.13	
PU-ZrP-B2	99.4	0.6	1.05				25.03	279.98	
PU-ZrP-B3	99.4	0.6	1.20				26.15	262.71	
PU-ZrP-B4	99.4	0.6	1.50				38.41	260.60	
PU-ZrP-B5	99.4	0.6	1.60				32.23	261.34	
PU-ZrP-B6	99.4	0.6	1.70				25.48	259.03	
PU-ZrP-B7	99.4	0.6	1.80				22.31	258.93	
PU-ZrP-B8	99.4	0.6	2.00				21.90	262.37	

Thermal analyses

Thermogravimetric (TGA) and differential thermogravimetry (DTG) analyses of the PU-ZrPn films were carried out on a TA-STDQ600 (TA Instruments Inc., New Castle, USA). The thermograms were acquired between 0°C and 500°C at a heating rate of 10°C/min. Nitrogen was used as the purge gas at a flow rate of 20 mL/min. An empty pan Al_2O_3 was used as a reference.

Differential Scanning Calorimetry (DSC) analysis of the PU, PU-ZrP4, PU-ZrP6′PU-ZrP8 and PU-ZrP16 composite films was carried on a NETZSCH DSC 200 F3 (Netzsch Co, Selb/Bavaria, Germany). Nitrogen at a rate of 20 mL min^{-1} was used as the purge gas. Aluminum pans containing 2–3 mg of film were sealed with pierced lid using the DSC sample press. All samples were preheated with a scan rate of 20°C/min over a temperature range of −30 to 250°C.

Mechanical properties

The tensile strength and elongation at break of all the composite films were determined using a Microelectronics Universal Testing Instrument Model Sans 6500 (Shenzhen Sans Testing Machine Co. Ltd., Shenzhen, China) according to the Chinese standard method (GB 13022-91). The films were cut into 10 mm wide and 100 mm long strips and mounted between cardboard grips (150 × 300 mm^2) using adhesive so that the final area exposed was 10 × 50 mm^2. The cross-head speed was 10 mm/min. All measurements were performed on three specimens and averaged.

RESULTS AND DISCUSSION

Fourier transform infrared spectroscopy

The FTIR spectra of PU, PU-ZrP4, PU-ZrP6, PU-ZrP8, and PU-ZrP16 films are shown in Figure 1. For the neat polyurethane film (PU), the band centered at 3291 cm^{-1} was due to the self-associate bonded *N*-H stretching.[26–28] A sharp peak near 1696 cm^{-1} was due to the C=O stretching vibrations.[29–32] The band at 1597 cm^{-1} was the C=C bending.[27] The peak at 1219 cm^{-1} was due to C—C=O peaks. Compared with the neat PU film, the composite films showed that the peak at 1696 cm^{-1} shifted gradually to higher wavenumber for PU-ZrP4 and PU-ZrP6 with an increase of α-ZrP loading, implying that there are hydrogen bonding interactions between the amino groups, carbonyl groups of PU and the hydroxyl groups of α-ZrP. Moreover, the hydrogen bonding N-H stretching ($\nu_{NH} \sim 3291 cm^{-1}$) absorption of PU also shifted slightly to higher wavenumber in the composite films.[28] This implies that the original intermolecular and intramolecular hydrogen bonding involved in films were destroyed due to the interactions between the carbonyl groups, amino groups of PU and α-ZrP, which improved the compatibility between them.[33]

X-ray diffraction

The XRD patterns of α-ZrP and PU-ZrPn films are shown in Figure 2. The first peak at $2\theta = 11.6°$ of α-ZrP indicates (001) reflections of α-ZrP. The interlayer

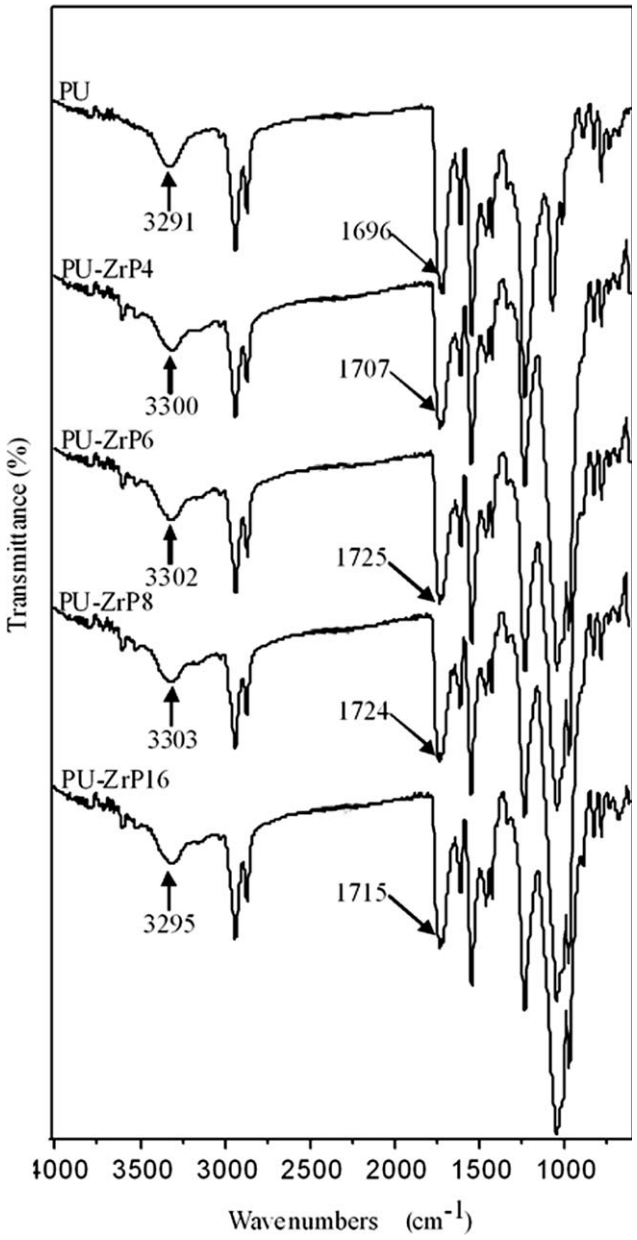

Figure 1 FTIR spectra of PU, PU-ZrP4, PU-ZrP6, PU-ZrP8, and PU-ZrP16 blend films.

distance in the (001) direction is estimated from Bragg's law, $2d\sin\theta = \lambda$, which is 7.4E. The neat polyurethane film (PU) showed a broad diffraction commencing from 12 to 28° in 2θ with lower magnitude. This indicates the amorphous nature of polyurethane, similar to other works.[34,35] The PU-ZrPn films showed the different XRD patterns as the neat PU film.[36–38] The characteristic diffraction peaks in the (001) direction for α-ZrP were found in the composites, and their diffraction peaks shifted to lower angle, which indicated that the polyurethane molecular chain intercalated the α-ZrP interlayer inducing the increase of the interlayer distance. It can be explained that the urethane linkages in castor oil-based polyurethane can serve as H-bond acceptor and donor, while α-ZrP has the hydroxyl group, leading to the formation of the hydrogen bonding interactions between the PU and the α-ZrP.[17,18,39] Meanwhile, all of the diffraction peaks for α-ZrP were found in PU-ZrP10 and PU-ZrP16 and the diffraction peaks of α-ZrP in PU-ZrP16 were identical with that of α-ZrP, indicating that α-ZrP aggregates evidently in the PU matrix with the increase of α-ZrP loading, which resulted in the profound decrease of composite mechanical properties in higher α-ZrP loading.

Also the crystal size D of (001) direction for α-ZrP in the composites was calculated by Scherrer's law, $D = k\lambda/\beta\cos\theta$[40–42] and listed in Table I. With the increase of α-ZrP loading, the minimum of D value appeared in PU-ZrP6 composite. This could be explained that the α-ZrP particles were dispersed

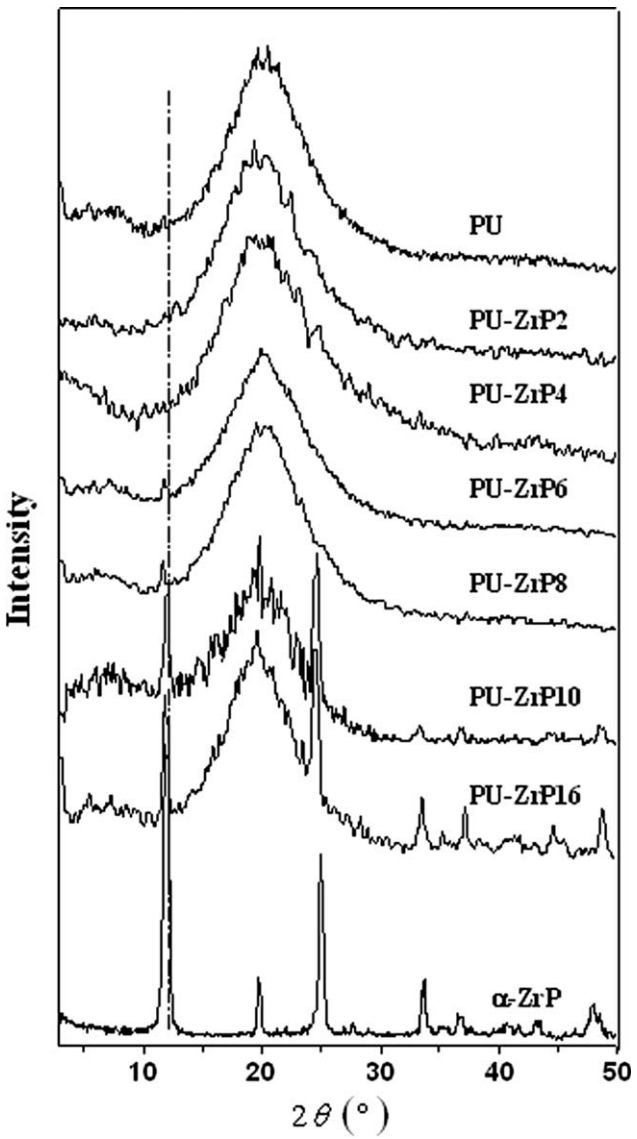

Figure 2 XRD patterns of α-ZrP and PU-ZrPn composite films.

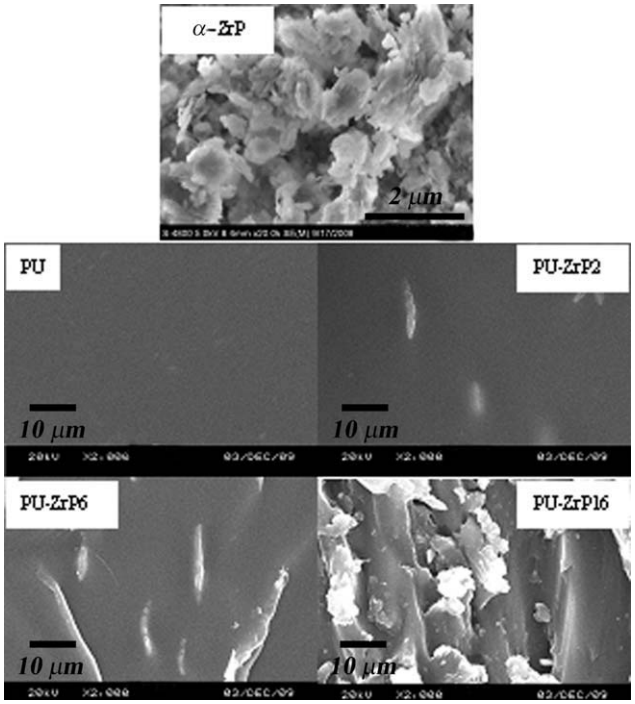

Figure 3 SEM images of the failure surfaces for α-ZrP and the PU, PU-ZrP2, PU-ZrP6, and PU-ZrP16 composite films.

best in PU-ZrP6 among all these composites, which resulted in the best mechanical properties for PU-ZrP6 composite.

Scanning electron microscopy and transmission electron microscopy

The morphological images of the PU-ZrPn composites and α-ZrP were studied by SEM, as shown in Figure 3. The α-ZrP shows a plate-like structure and regular cubic sheets. As compared to the matrix, the morphology of α-ZrP can be easily identified. The white substance in the images corresponds to α-ZrP on the fractured surface of the composites. Well-dispersed α-ZrP in the composites can be observed in PU-ZrP2 and PU-ZrP6, while in the PU-ZrP16, it is found that different sizes of α-ZrP aggregates or chunks disorderly on the surface of the PU, implying that the mechanical properties could become worse when the α-ZrP loading are 1.6 wt %. The images from SEM implied that α-ZrP fillers are dispersed and inlayed well and regularly in PU matrix for PU-ZrP2 and PU-ZrP6. To observe the microstructure of composite, the TEM micrographs of the PU matrix and PU-ZrP6 composite are shown in Figure 4. The neat PU exhibits a uniform microstructure. For PU-ZrP6 composite, the dark particles correspond to the individual α-ZrP platelets in the PU matrix. The layered α-ZrP in the aspect ratio of about 20 are randomly and well dispersed in the PU

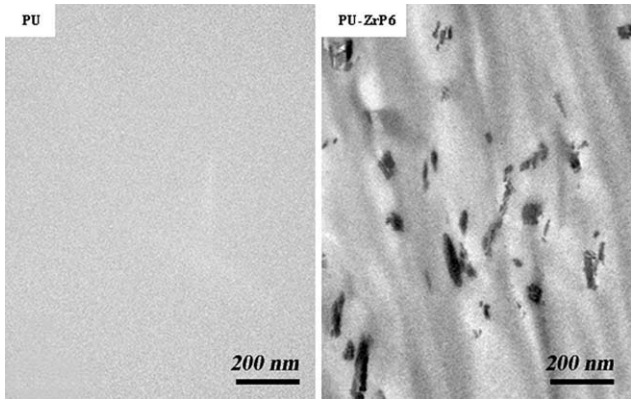

Figure 4 TEM micrographs of PU matrix and PU-ZrP6 composite film containing 0.6 wt % α-ZrP.

matrix without apparent interface separation, which resulted from strong interaction between α-ZrP and PU.[34] The microstructure from SEM and TEM benefit the formation intermolecular hydrogen bonding and increase the molecular interaction. Such an even and uniform distribution of the fillers in the PU matrix played an important role in improving the mechanical performance of the films as discussed later.

Thermal analysis

The thermal stability for the neat PU and composite films is studied by thermogravimetric analysis (DTG) shown in Figure 5. First, the weight loss between 217 and 336°C was attributed to the breaking of urethane bond.[35,43,44] Second, the decomposition stage of polyurethane lies in the range from 336 to 480°C, due to castor oil molecules resulted in a faster rate of weight loss. This was accorded with literature.[45] The summary of TGA results was listed in Table I. The temperatures of maximum loss ratio

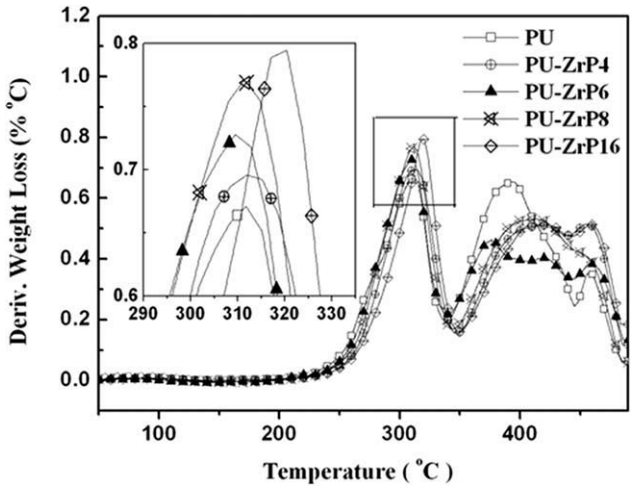

Figure 5 DTG curves of pure PU, PU-ZrP4, PU-ZrP6, PU-ZrP8, and PU-ZrP16 composite films.

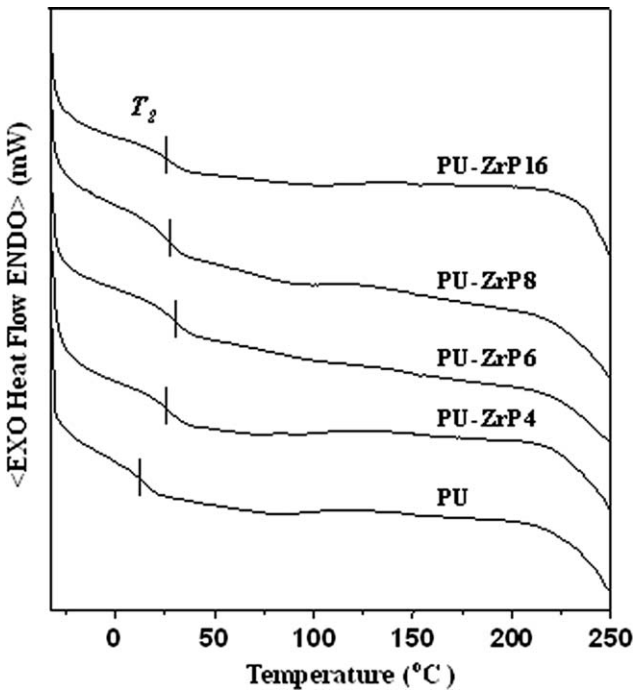

Figure 6 DSC curves of pure PU, PU-ZrP4, PU-ZrP6, PU-ZrP8, and PU-ZrP16 composite films.

(T_{max}) was obtained from DTG curve. It was seen that T_{max} of neat PU film were 311.6°C. Compared with the T_{max} of neat PU film, it was seen that the T_{max} of all composite films was hardly changed with low α-ZrP loading in PU matrix (Table I). However, the integral procedural decomposition temperature (IPDT)[46] of the composite improved with increased α-ZrP loading, and a maximum value of 333.23°C achieved. The thermal stability improved can be explained through the reduced mobility of the PU chains in the composite, which benefits from the stronger hydrogen bonding interaction and the intercalation of the PU molecule into the layer space. Because of reduced chain mobility, the degradation process will be slowed and decomposition will take place at higher temperatures.[47]

Figure 6 shows the DSC curves for the films PU, PU-ZrP4, PU-ZrP6′PU-ZrP8, and PU-ZrP16. One glass transition was detected in the composite films. Generally, the T_g was influenced by many factors, such as dispersion and arrangement of α-ZrP in polymer matrix and α-ZrP loading in composite films.[48] The T_g temperature associated with the glass transition of PU for the composite films PU-ZrP4, PU-ZrP6′PU-ZrP8, and PU-ZrP16 were listed in Table I, which were higher than that of the neat PU film (18.40°C). The results indicate that the stronger interactions between PU and α-ZrP prevented the segmental motion of polymer chains, consequently, the T_g will take place at higher temperature. Additionally, with an increase α-ZrP loading, the

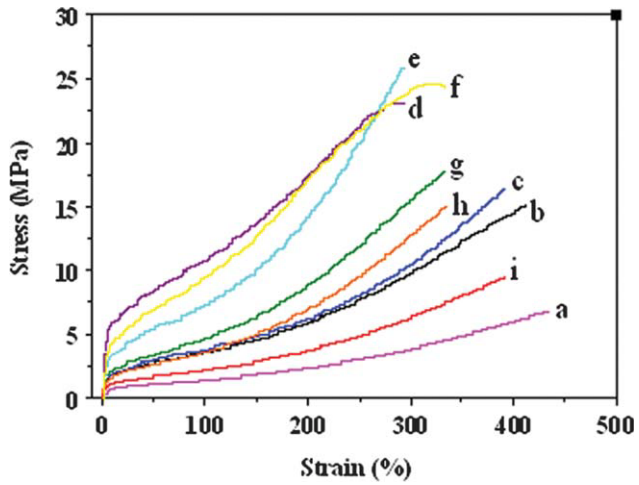

Figure 7 Stress-strain curves of (a) pure PU and PU/α-ZrP composites with (b) 0.2 wt %, (c) 0.4 wt %, (d) 0.5 wt %, (e) 0.6 wt %, (f) 0.7 wt %, (g) 0.8 wt %, (h) 1.0 wt %, and (i) 1.6 wt % of α-ZrP, respectively. [Color figure can be viewed in the online issue, which is available at wileyonlinelibrary.com.]

composites' T_g increased at the beginning and then decreased slightly. The reason for this phenomenon can be attributed to the aggregation of α-ZrP particles at higher loadings from 0.8 wt % to 1.6 wt %.

Mechanical properties

Mechanical properties of the composite films with different α-ZrP loading were investigated by tensile testing. From the stress–strain curves in Figure 7, two regions of deformation behavior of all samples were observed. In the First Newton Area, the stress increased rapidly with the increase in strain at low strains, and the stress increased regularly at higher strain with the strain increasing up to the break of the films in the High-elastic zone.[25] It is worth noting that all samples displayed clearly elastomeric

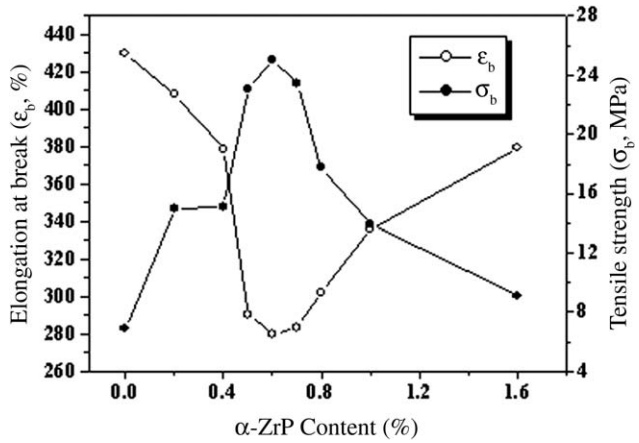

Figure 8 The mechanical properties of PU, PU-ZrP2, PU-ZrP4, PU-ZrP5, PU-ZrP6, PU-ZrP7, PU-ZrP8, PU-ZrP10, and PU-ZrP16 composite films.

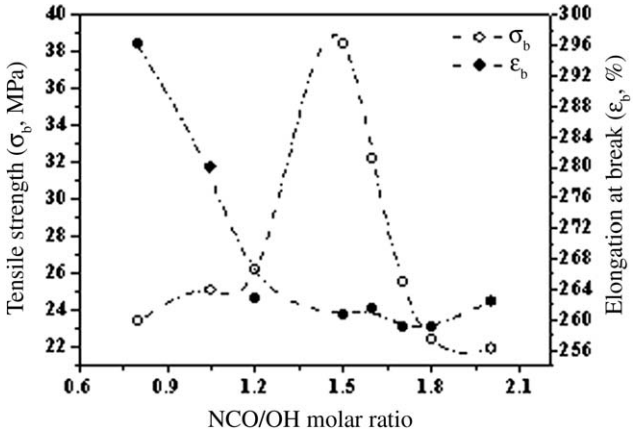

Figure 9 Mechanical properties (σ_b and ε_b) of the PU-ZrP-B1, PU-ZrP-B2, PU-ZrP-B3, PU-ZrP-B4, PU-ZrP-B5, PU-ZrP-B6, PU-ZrP-B7, and PU-ZrP-B8 composite films as a function of NCO/OH molar ratios.

behavior. The area of under the stress-strain curve can be used as a measurement of the material toughness. The relatively large area of under the stress–strain curve for the films PU-ZrP4 and PU-ZrP6 indicated a character of toughened rubber. Results for tensile strength and elongation at break of all samples were presented in Figure 8. It was observed that the tensile strength (σ_b) significantly increased from 6.91 MPa to 25.03 MPa when the α-ZrP loading levels increased from 0 to 0.6 wt %, while the elongation at break (ε_b) reduced from 430.14% to 279.98%. When the α-ZrP loading levels were greater than 0.8 wt %, the tensile strength of the composite films decreased. Conversely, the elongation at break decreased for all of the tested samples compared with the PU matrix, with a maximum decrease at 0.6 wt %. The reseans result from the stronger hydrogen bonding interaction between —OH groups of α-ZrP and the —NH_2 and —C=O of PU. Meanwhile, the decrease of the mechanical strength of the films with greater than 0.6 wt % may be attributed to the aggregation of excess filler in PU matrix. In combination with the result of SEM, it can be summarized that an optimum α-ZrP loading levels exists for an effective enhancement of the mechanical property of the composites. The dispersion of α-ZrP with lower loading levels in PU matrix was uniform and preferable, indicating the best interaction between the PU and α-ZrP due to the stronger hydrogen bonding. Hence, it results in the improved mechanical property. However, with the greater α-ZrP loading levels, the agglomerates of α-ZrP can damage the structure of the matrix, which results in mechanical property decrease.

The effects of NCO/OH molar ratio on σ_b and ε_b of PU-ZrP-Bn composite films are shown in Figure 9. With an increase of NCO/OH molar ratio, ε_b values of the films decreased with higher tensile strength at break, a maximum value of σ_b achieved at 1.5 of NCO/OH molar ratio for PU-ZrP-B4, resulting from the relative high chemical crosslinking that can restrict the chain mobility and increase the intermolecular attraction of hard to hard-segments.

CONCLUSIONS

A series of composite films that consisted of PU and layered α-ZrP were prepared by a solution casting method. The results from XRD and SEM indicated that the PU and α-ZrP possess good miscibility, which results from hydrogen bonding ineraction between —OH groups of α-ZrP and the —NH_2 and —C=O of PU. Compared with the tensile strength of the neat PU, it can be seen that the tensile strength of the composite films increased by 556.0% with 0.6 wt % α-ZrP loading levels at 1.5 NCO/OH molar ratios. The results from tensile testing and TGA indicated that the zirconium phosphate favored the polymer mechanical properties and the thermal stability with lower α-ZrP loading levels.

References

1. Hatti-Kaul, R.; Törnvall, U.; Gustafsson, L.; Börjesson, P. Trends Biotech 2007, 25, 119.
2. Campanella, A.; Bonnaille, L. M.; Wool, R. P. J Appl Polym Sci 2009, 112, 2567.
3. Deka, H.; Karak, N. Progr Org Coat 2009, 66, 192.
4. Fritzen-Garcia, M. B.; Oliveira, I.; Zanetti-Ramos, B. G.; Fatibello-Filho, O.; Soldi, V.; Pasa, A. A. Sensors Actuators, B: Chem 2009, 139, 570.
5. Sharna, V.; Kundu, P. P. Progr Polym Sci 2008, 33, 1199.
6. Xu, Y.; Petrovic, Z.; Das, S.; Wilkes, G. L. Polym 2008, 49, 4248.
7. Hablot, E.; Zheng, D.; Bouquey, M.; Avérous, L. Macromol Mater Eng 2008, 293, 922.
8. Petrovic, Z. S. Polym Rev 2008, 48, 109.
9. Javni, I.; Zhang, W.; Petrovic, Z. S. J Appl Polym Sci 2003, 88, 2912.
10. Somani, K. P.; Kansara, S. S.; Patel, N. K., Rakshit, A. K. Int Jadhes Adhes 2003, 23, 269.
11. Bai, S.; Khakhar, D. V.; Nadkarni, V. M. Polym 1997, 38, 4319.
12. Mortley, A.; Bonin, H. W.; Bui, V. T. Nucl Instrum Meth B 2007, 265, 98.
13. Herrera-Alonso, J. M.; Marand, E.; Little, J. C.; Cox, S. S. J Membr Sci 2009, 337, 208.
14. Zhang, R.; Dowden, A.; Deng, H.; Baxendale, M.; Peijs, T. Compos Sci Technol 2009, 69, 1499.
15. Sabzi, M.; Mirabedini, S. M.; Zohuriaan-Mehr, J.; Atai, M. Prog Org Coatings 2009, 65, 222.
16. Finnigan, B.; Martin, D.; Halley, P.; Truss, R.; Campbell, K. Polym 2004, 45, 2249.
17. Yang, Y. J.; Liu, C. H.; Wu, H. X. Polym Test 2009, 28, 371.
18. Wu, H. X.; Liu, C. H.; Chen, J. G.; Chang, P. R.; Chen, Y.; Anderson, D. P. Carbohydrate Polyp 2009, 77, 358.
19. Clearfield, A.; Dual, W. L.; Medina, A. S.; Smith, G. D.; Thomas, J. R. J Phys Chem 1969, 73, 3224.
20. Clearfield, A.; Medina, A. S.; Dual, W. L.; Graces, J. M. J Inure Null Chem 1972, 34, 329.
21. Clearfield, A.; Jerks, P. J Inure Null Chem 1981, 43, 2117.
22. Sun, L. Y.; Boo, W. J.; Browning, R. L.; Clearfield, A. J Chem Mater 2005, 179, 5606.

23. Jung, J. H.; Son, H. J Micro Porous Malodorous Mater 2007, 106, 49.
24. Sun, L. Y.; Boo, W. J.; Sue, H. J.; Clearfield, A. New J Chem 2007, 31, 39.
25. Zhou, Q.; Zhang, L. N.; Zhang, M.; Wang, B.; Wang, S. Polym 2003, 44, 1733.
26. Berta, M.; Lindsay, C.; Pans, G.; Camino, G. Polym Degrad Stab 2006, 91, 1179.
27. Nakamura, K.; Nishimura, Y.; Zetterlund, P.; Hatakeyama, T.; Hatakeyama, H. Thermochimi Acta 1996, 282, 433.
28. Liu, J.; Ma, D.; Li, Z. Eur Polym Mater 2002, 38, 661.
29. Stuart, L.; Cooper, A. V. J Appl Polym Sci 1966, 10, 1837.
30. Jeffrey, T.; Koberstein1, I. G.; Thomas, C. C. J Appl Polym Sci Part B: Polym Phys 1986, 24, 2487.
31. Kuana, H. C.; Maa, C. C. M.; Changa, W. P.; Yuena, S. M.; Wub, H. H.; Lee, T. M. Compos Sci Technol 2005, 65, 1703.
32. John, J.; Bhattacharya1, M.; Turner, R. B. J Appl Polym Sci 2002, 86, 3097.
33. Cervantes-Uc, J. M.; Moo Espinosa, J. I.; Cauich-Rodriguez, J. V.; Avila-Ortega, A.; Vazquz-Torres, H.; Marcos-Fernandez, A.; San Roman, J. Polym Degrad Stab 2009, 94, 1666.
34. Salahuddin, N.; Abo-El-Enein, S. A.; Selim, A.; Salah El-Dien, O. Appl Clay Sci 2010, 47, 242.
35. Semenzato, S.; Lorenzetti, A.; Modesti, M.; Ugel, E.; Hrelja, D.; Besco, S.; Michelin, R. A.; Sassi, A.; Facchin, G.; Zorzi, F.; Bertani, R. Appl Clay Sci 2009, 44, 35.
36. Furuakwa, M. J Appl Polym Sci, Appl Polym Symp 1994, 53, 61.
37. Furukawa, M. Angewante Macromol Chemie 1997, 252, 33.
38. Furukawa, M.; Shiiba, T.; Murata, S. Polymer 1999, 40, 1791.
39. Wu, H.; Liu, C.; Chen, J.; Yang, Y.; Chen, Y. Polym Int 2010, 59, 923.
40. Kar-Gupta, R.; Venkatesh, T. A. Acta Mater 2008, 56, 3810.
41. Shen, L.; Chen, Z. Int J Solids Struct 2007, 44, 3379.
42. Byun, S. C.; Jeong, Y. J.; Park, J. W.; Kim, S. D.; Ha, H. Y.; Kim, W. J. Solid State Ionics 2006, 177, 3233.
43. Shen, Z.; Simon, G. P.; Cheng, Y. B. J Appl Polym Sci 2004, 92, 2101.
44. Jasin'ska, L.; Haponiuk, J. T.; Balas, A. J Therm Anal Calorim 2008, 93, 777.
45. Zhang, L.; Huang, J. J Appl Polym Sci 2001, 80, 1213.
46. Park, S. J.; Kim, H. C. J Polym Sci Part B: Polym Phys 2001, 39, 121.
47. Kuljanin, J.; îComor, M. I.; Djokovíc, V.; Nedeljkovíc, J. M. Mater Chem Phys 2006, 95, 67.
48. Xiong, J.; Liu, Y.; Yang, X.; Wang, X. Polym Degrad Stab 2004, 86, 549.